Pharm Res (2014) 31:2124–2139
DOI 10.1007/s11095-014-1313-7

RESEARCH PAPER

Zinc Protoporphyrin Polymeric Nanoparticles: Potent Heme Oxygenase Inhibitor for Cancer Therapy

Hasti Rouhani • Nima Sepehri • Hamed Montazeri • Mohammad Reza Khoshayand • Mohammad Hossein Ghahremani • Seyed Nasser Ostad • Fatemeh Atyabi • Rassoul Dinarvand

Received: 19 September 2013 / Accepted: 23 January 2014 / Published online: 21 February 2014

ABSTRACT

Purpose Oxidation therapy is an antitumor strategy in which, apoptosis or necrosis is caused by either excess delivery of reactive oxygen species (ROS) as an oxidant or anti-oxidant inhibition. Heme oxygenase (HO) is an anti-oxidant enzyme that plays an important role in cell growth and proliferation. The purpose of this study was to prepare poly lactic-co-glycolic acid (PLGA) nanoparticles (NPs) loaded with zinc protoporphyrin (ZnPP) to deliver the HO inhibitor into tumor.

Methods PLGA NPs were prepared using nanoprecipitation technique and their characteristics were optimized by Box-Behnken experimental design. Scanning electron microscopy and *in vitro* studies consisting of drug release, HO inhibitory effect, cytotoxicity and cellular uptake followed by *in vivo* biodistribution and blood cytotoxicity were carried out. Internalization of coumerin-6 loaded NPs by PC3 cells was visualized by confocal laser scanning microscopy beside quantitatively analysis.

Results NPs average size, entrapment efficiency and drug loading were 100.12 ± 5.345 nm, $55.6\% \pm 2.49$ and $7.98\% \pm 0.341$ respectively. Equal HO inhibitory effect of NPs compared to free ZnPP was observed. The IC_{50} value of ZnPP-NPs for PC3 human prostate cancer cells was found to be 2.14 ± 0.083 μM.

Conclusion In conclusion, ZnPP loaded PLGA NPs could exhibit enough HO inhibitory effect against cancer cells to be considered as a promising candidate for cancer treatment investigation.

KEY WORDS anti-cancer · heme oxygenase inhibition · PLGA nanoparticles · reactive oxygen species · zinc protoporphyrin

ABBRIVIATIONS

ALT	Alanine aminotransferase
AST	Aspartate aminotransferase
BUN	Blood Urea Nitrogen
CLSM	Confocal laser scanning microscopy
Cr	Creatinine
DL	Drug loading
DMSO	Dimethyl sulfoxide
EE	Entrapment efficiency
FBS	Fetal Bovine Serum
Hb	Hemoglobin
HO	Heme oxygenase
LDH	Lactate dehydrogenase
MTT	3-(4,5-dimethylthiazol-2-yl)-2,5-diphenyl tetrazolium bromide
NADPH	Nicotinamide adenine dinucleotide phosphate
NPs	Nanoparticles
PBS	Phosphate buffer saline
PDI	Poly Dispersity Index
PLGA	Poly lactic-co-glycolic acid
RBC	Red Blood cells
ROS	Reactive Oxygen Species

H. Rouhani • N. Sepehri • F. Atyabi • R. Dinarvand
Department of Pharmaceutics, Faculty of Pharmacy
Tehran University of Medical Sciences, Tehran, Iran

H. Rouhani • N. Sepehri • F. Atyabi • R. Dinarvand (✉)
Nanotechnology Research Centre, Faculty of Pharmacy
Tehran University of Medical sciences, Tehran, Iran
e-mail: dinarvand@tums.ac.ir

H. Rouhani • N. Sepehri
Nano Alvand Co., Avicenna Tech. Park
Tehran University of Medical Sciences, Tehran, Iran

H. Montazeri
Department of Molecular Biology, Pasteur Institute of Iran, Tehran, Iran

M. R. Khoshayand
Department of Drug and Food Control, Faculty of Pharmacy and
Pharmaceutical quality assurance Research Center
Tehran University of Medical Sciences, Tehran, Iran

M. H. Ghahremani • S. N. Ostad
Department of Toxicology-Pharmacology, Faculty of Pharmacy
Tehran University of Medical Sciences, Tehran, Iran

RPMI	1640 Roswell Park Memorial Institute medium
SEM	Scanning electron microscopy
WBC	White Blood Cells
ZnPP	Zinc protoporphyrin IX (ZnPP)

INTRODUCTION

In recent years, many studies have been carried out to explore the cause of cancer cell development, to improve anticancer drugs efficacy, and to reduce cancer therapies correlated side effects (1,2). Among the numerous proposed mechanisms, oxidative stress is a well-known process that is critical for cancer cell growth (3,4). The balance between oxidant and anti-oxidant species in normal cells plays an important role in normal metabolism, signal transduction and regulation of cellular functions. The disturbance in oxidant and anti-oxidant balance is known as oxidative stress (5). Reactive oxygen species (ROS) are oxygen containing oxidizing agents including free radicals (superoxide radicals $O_2^{\cdot -}$) and non-radical (hydrogen peroxide H_2O_2) species of oxygen. ROS is the product of normal cellular metabolism (6). Despite the fact that, it is essential for signal transduction pathways, it is highly reactive and an increase in ROS level is harmful to the cell. In normal conditions, the balance in the intracellular ROS level is regulated by the aid of anti-oxidant defense components. On the other hand, cancer cells are under increased and persistent oxidative stress due to elevated levels of intracellular ROS generation and low level of anti-oxidants. However, this amount of oxidative stress in cancer cells is insufficient to cause apoptosis or necrosis (7,8).

Since the cancer cells are under high levels of oxidative stress compared to normal cells (9,10) and with regarding the hazardous effects of ROS, an antitumor strategy named "oxidation therapy" has been developed. This strategy is based upon two concepts: first, induction of excess oxidative stress in tumor cells and second, disruption of the anti-oxidative defense systems including small ROS scavengers, inhibitors of ROS generating enzymes and anti-oxidative enzymes (11–13).

Heme oxygenase (HO) is known as an anti-oxidant enzyme that catalyzes the degradation of heme to form biliverdin, iron and carbon monoxide. Biliverdin is promptly reduced to the potent antioxidant bilirubin by biliverdin reductase (8,14). There are three known isoforms of HO, among which HO-1 is an inducible isoform and is activated in response to oxidative stress such as ROS. It has been found that HO-1 is expressed in various tumor cells. HO-1 stimulates cell growth and proliferation by its cytoprotective functions including regulation of oxidative stress and anti-apoptotic effects. On the basis of these concepts, delivery of HO-1 inhibitors into tumor tissue is considered as a new strategy in cancer therapy (15).

The inhibitory effects of HO and essentially the antitumor activity of Zinc protoporphyrin IX (ZnPP) have been studied widely (16–22). ZnPP is classified as a metalloporphyrin compound, in which the central iron of porphyrin ring in heme is replaced with zinc. The use of ZnPP as an injectable formulation is limited due to its very low solubility. In addition, the necessity of efficient delivery of HO inhibitors to tumor tissue is inevitable, since the non-specific inhibition of HO may cause various side effects in normal cells by reducing the favorable effects of normal anti-oxidants (11,23).

In this context, nanotechnology based systems for delivery of anticancer drugs with a lower toxicity in normal cells and higher efficiency in cancer cells have been developed (24). The importance of polymeric nanoparticles (NPs) for the delivery of anti-cancer agents has grown extensively (25). Among polymers, poly lactide-co-glycolide (PLGA) is biocompatible, biodegradable polyester being regarded as FDA approved for human use. Hence, it has been in the center of focus for developing drug loaded NPs in cancer therapy (26). Development of PLGA NPs can be a good strategy for achieving an efficient and a selective delivery of ZnPP to tumor sites by a sufficient ZnPP loading parallel to maintaining the HO inhibitory properties.

The current study presents the development of ZnPP encapsulated PLGA nanoparticles by nanoprecipitation method followed by the Box-Behnken experimental design to optimize the formulations based on their mean particle size, entrapment efficiency and drug loading. Furthermore, the optimized NPs were characterized for their shape, morphology and *in vitro* drug release. The HO inhibitory effect of ZnPP-NPs in comparison with free ZnPP was assessed. Moreover, the *in vitro* cytotoxicity against PC3 human prostate cancer cells in addition cellular internalization and the *in vivo* biodistribution of NPs were reported.

MATERIALS AND METHODS

Zinc protoporphyrin IX was purchased from Alexis Biochemical (CA, USA). Poly lactide-co-glycolide (PLGA; lactide: glycolide, 50:50; Resomer RG 504H, molecular weight 48,000) was purchased from Boheringer Ingelheim (Ingelheim, Germany). β-Nicotinamide adenine dinucleotide 2′-phosphate (NADPH), coumarin-6, hemin and 3-(4,5-dimethylthiazol-2-yl)-2,5-diphenyl tetrazolium bromide (MTT), were purchased from Sigma Aldrich (St. Louis, MO, USA). Roswell Park Memorial Institute medium (RPMI 1640), Fetal Bovine Serum (FBS), penicillin and streptomycin were obtained from Life technologies (Grand Island, NY, USA). PC3, human prostate cancer cell line was obtained from American Type Culture Collection (ATCC). Dimethyl sulfoxide (DMSO) was obtained from Merck (Darmstadt, Germany).

Nanoparticles Preparation

NPs were prepared by a nanoprecipitation technique. Typically, different amounts of PLGA and ZnPP were dissolved in 1 ml DMSO. The organic phase was added slowly into water as non-solvent under stirring. NPs were then recovered by centrifugation at 19,000×g for 30 min at 10°C (Sigma, 3–30 k, Germany) and were washed thereafter three times with water to remove DMSO. NPs suspensions were freeze dried (Christ, alpha 2-4 LD plus, Germany) to improve their stability for further studies and analyses. To find out a suitable cryoprotectant that has the minimum effect on the NPs characteristics, sucrose, glucose and mannitol were employed in different concentrations (0.5, 1, 2, 3, 4, 5% w/v). NPs suspension without or with different cryoprotectants were added to glass vials and were frozen at −18 to −20°C. After almost 8 h, the frozen suspension of NPs were freeze dried for 48 h including primary drying (30 h at −40°C) and secondary drying (18 h at −30°C) processes under 0.07 mbar vacuum. The freeze dried vials were fully stoppered and stored at room temperature.

NPs characteristics such as size, poly dispersity Index (PDI), zeta potential, entrapment efficiency (EE) and drug loading (DL) were measured in the absence or presence of the cryoprotectants, both before and after freeze drying. Besides, the appearance of the freeze-dried cake and the ease of reconstitutions were studied. The most suitable cryoprotectant was used for further studies.

Experimental Design

Selected parameters of the nanoprecipitation method such as stirring rate, polymer concentration and non-solvent volume were evaluated in preliminary studies to find the effective factors with suitable levels for optimization studies. By choosing the other parameters constant, NPs were prepared with different stirring rates range of 700–1,400 rpm, polymer concentration range of 5–40 mg/ml and non-solvent volume range of 5–40 ml. Resulting NPs were characterized with respect to their size, PDI, EE and DL.

The formulation parameters were statistically optimized using Box-Behnken design. Based on preliminary studies, stirring rate (900 rpm) was held constant and the effect of three independent variables including drug amount (X1), polymer amount (X2) and non-solvent volume (X3) on mean particle size, EE and DL as response variables was studied in this design. As shown in Table I this design had three levels per factors as −1, 0 and +1. The experimental design included a total of 17 experiments. NPs were prepared following the described method. Each experiment was done thrice and the resultant data was analyzed by Design- Expert® software (V.7.0.0, State-Ease, Inc., Minneapolis, USA)

Table I Levels of Design Variables Investigated in the Box-Behnken Design

Independent variables	Levels		
	−1	0	+1
Polymer amount (mg)	10	17.5	25
Drug amount (mg)	1	1.75	2.5
Non-solvent volume (ml)	5	22.5	40

Characterization of Nanoparticles

Particle Size, PDI and Zeta Potential

The freeze dried nanoparticles were dispersed in distilled water. Samples were diluted 10 times with distilled water. The average of particle size, size distribution indicated by PDI and zeta potential were measured by dynamic light scattering (Malvern Zetasizer ZS, Worcestershire, UK). The mean value of three samples was finally reported.

Drug Content

Drug content was expressed by two definitions; drug loading as the fraction of drug amount to the whole weight of the nanoparticles and drug entrapment efficiency as the relative mass of ZnPP in NPs to the mass of drug used in the formulation. For this purpose, sufficient amount of lyophilized NPs was dissolved in DMSO. Quantification of ZnPP in the solution was made by UV-spectrophotometery (Cecil 9,000, Cecil Instruments Ltd, Cambridge, UK) at 423 nm using calibration curve obtained from ten different ZnPP concentrations in a range of 0.065 to 1 μg/ml.

NPs Morphology by Scanning Electron Microscopy (SEM)

The particle morphology was analyzed by scanning electron microscopy (SEM, S4160, Hitachi, Japan). A suspension of NPs was spread on an aluminum stub and was allowed to be dried afterwards. The samples were then coated with a thin layer of gold under vacuum condition using a sputter coater (SCD005, Bal-Tec, Switzerland).

In Vitro Release Rate of ZnPP from the NPs

For this study, the optimized NPs contained almost 8% w/w drug loading were used. Nine mg of NPs were inserted in centrifuge tubes and were dispersed in 25 ml phosphate buffer saline (PBS) (10 mM) with pH 7.4 and pH 5.2 to simulate the lower pH condition of cancer cells. The tube was incubated for several days at 37°C under dark condition with mild agitation. At programmed time intervals, the tubes were centrifuged at 17,000×*g* for 15 min to precipitate the NPs. The

supernatant was collected for further analyses and the equal volume of withdrawn solution was replaced with fresh PBS to redisperse the pellet. The released amount of ZnPP in the samples was quantified by UV-spectrophotometery in 423 nm wavelength. The study was performed in three separate experiments and the mean values were reported.

X-ray Diffraction (XRD)

X-ray diffraction pattern of the samples were collected using X-ray diffractometer (Siemens 85, Germany) with Cu Kα radiation generated. Powder of free ZnPP, PLGA, lyophilized ZnPP-NPs and physical mixture of ZnPP and PLGA were filled to the sample holder and scanned with 2Θ range of 3–90° and step size of 0.04 (2°Θ).

In Vitro HO Inhibitory Effect Test

The inhibitory effect of HO activity by ZnPP in different formulations was investigated in spleen and liver preparations of rats (provided by animal care center, Faculty of Pharmacy, Tehran University of Medical Sciences). HO assay was performed by a modification to the previous reported procedure by Maines (27). For this purpose, rats were fasted for 12 h with free access to water. The animals were then sacrificed by decapitation and their spleen and liver were homogenized after the addition of 2 fold volumes of potassium phosphate buffer (pH 7.4, 10 mM). The resulting homogenates were centrifuged at 5,000×*g* for 30 min to remove the cell debris and the supernatant fractions were then centrifuged at 105,000×*g* for 1 h by ultracentrifuge (Beckman Coulter, Optima MAX-XP, CA, USA). The liver supernatant fraction (liver cytosolic fraction) was used as the source of biliverdin reductase and the HO enzyme was recovered in the pellet fraction of the spleen (splenic microsomal fraction) where the pellets were resuspended in potassium phosphate buffer. Protein contents of both liver cytosolic and spleen microsomal extraction was measured by Bradford assay (27,28).

HO activity was measured by mixing the proteins content of 1 mg spleen microsomal and 3 mg liver cytosol, 333 μM nicotinamide adenine dinucleotide phosphate (NADPH) with enzyme inhibitors in given concentrations to reach the final volume of 200 μL. The control sample was prepared the same way but no enzyme inhibitors were added to the sample. The activity of enzyme was initiated by addition of hemin (33 μM). After sufficient incubation time (15 min) in 37°C, the reaction was ended by addition of HCl 0.1 N (20 μL). Subsequently, bilirubin formation as a product of this reaction was quantified spectrophotometrically by the difference in absorbance at 450 and 560 nm using an extinction coefficient of 40 mM^{-1} cm^{-1} for bilirubin. For all experiments, the solutions were prepared immediately before usage and the experiments were performed triplicate.

Cellular Studies

In Vitro Cytotoxicity

The MTT assay was performed to study *in vitro* cytotoxicity in PC3 human prostate cancer cell line. Concisely, cells were cultivated in RPMI 1640 medium supplemented with 10% FBS and 1% penicillin-streptomycin at 37°C in a humidified atmosphere of 5% CO_2. 48 h before treatment, the cells were seeded in 96 well plates and when the cells were at 70% of population density, they were treated with either free ZnPP (stock solution in DMSO diluted with culture media) or ZnPP NPs suspensions at a designated equivalent ZnPP concentration ranging from 0.25 to 40 μM. 24 and 48 h after treatment, cell mediated toxicity was determined using MTT assay. To this end, 20 μl of 5 mg/ml MTT solution in PBS was added to each well. The plates were then incubated for 4 h in humidified incubator foil wrapped. Insoluble formazan precipitates solubilized by 60 μl DMSO. The relative absorbance was measured *via* plate reader (BioTek, ELx800, VT, USA) at 590 nm followed by background correction at 690 nm. Vehicle (DMSO solution in the same concentration of ZnPP solution) and blank (NPs without drug) in addition to untreated cells were used as control samples. It should be mentioned that, in all the experiments the percent of DMSO did not exceed from 0.5% of total volume. The viability was then expressed as the absorbance ratio of treated cells to control cells.

In Vitro Cellular Uptake of NPs

For quantitative study, the PC3 cells were seeded in fluorescence compatible plate. After 48 h, when the cells reached 70% confluency, the medium was replaced with coumarin-6 loaded NPs at concentration of 1.25 μg/ml and incubated for 0.5, 1, 2 and 4 h. Coumarin-6 loaded NPs were prepared following the described method for ZnPP-NPs. Untreated cells were used as control groups. At mentioned periods, the NPs suspension was removed and the wells were washed with 100 μl of cold PBS to remove the NPs which were not internalized. Next, 100 μl culture media was added followed by 50 μl Triton X-100 solution in 0.2 N NaOH to lyse the cells. The fluorescence intensity of each well was measured on microplate reader (BioTek, Synergy4, VT, USA) using 470 and 520 nm as excitation and emission wavelength, respectively. The percent of coumarin-6 detected in sample wells loaded with NPs was calculated to untreated cells and reported as percent cellular uptake.

To visualize the internalization of NPs by PC3 cell, confocal laser scanning microscopy (CLSM) (Nikon Ti Eclipse, Japan) was used to qualitatively evaluate the cellular uptake. PC3 cells were seeded in 6 well plates. 48 h later, when the cells reached 70% confluency, the medium was removed and

the cells were incubated with coumarin-6 loaded NPs for 4 h. The NPs suspension was then removed and each well was washed with PBS three times. The cells were then fixed by 20 min incubation with 1.5 ml 75% ethanol and observed under CLSM using a FITC filter.

In Vivo Studies

Animals

Adult balb/c mice, with a body weight between 25–30 g (provided by animal care center, Faculty of Pharmacy, Tehran University of Medical Sciences) were used for the investigations. Animal experiments were approved by the ethical committee of Pharmaceutical Research Centre, Tehran University of Medical Sciences.

Biodistribution Assay

Mice were randomly assigned into three discrete groups (five mice per group). Animals in each group were injected with 0.15 ml i.v. injection of either free ZnPP (in NaOH 0.2 N diluted with NaCl 0.9%) or ZnPP-NPs (in NaCl 0.9%) containing 5 mg/kg ZnPP or normal saline (as control group) via the tail vein. At various times after dosing, mice were sacrificed and major organs were collected for analyses. The blood samples were drawn from the inferior vena cava. The mice were fasted 8–12 h with free access to water before sacrificing.

The organ samples consisting of lungs, liver, heart, kidneys, intestine and spleen were removed and washed with PBS to remove surface blood. The organs were then weighed accurately and were homogenized in 3 ml PBS. The resulting homogenates as well as blood samples were centrifuged at 5,000×*g* for 10 min. Methanol was added in equal volume as that of the supernatant to precipitate the unwanted proteins and was centrifuged thereafter for 10 min at 5,000×*g*. The supernatant was assayed for ZnPP by spectrofluorophotometry (Shimadzu, Japan) at $\lambda_{ecitation}=420$ nm and $\lambda_{emission}=590.4$ nm. Calibration curve of ZnPP from six different concentrations was obtained afterwards in a range of 0.012 to 0.1 μg/ml for calculation processes. The acquired data were normalized with the control group, which received normal saline.

Hematological Toxicity

Mice were randomly assigned into two groups having three mice in each one. The mice in experiment group received ZnPP-NPs suspension that was prepared in NaCl 0.9% (150 μl of suspension corresponding to 10 mg ZnPP/kg). The control group received NaCl 0.9%. For each group, five animals were injected intravenously into the tail vein. The mice were fasted overnight but had free access to water, and were sacrificed in 24 and 48 h post administration.

Blood samples were obtained from the inferior vena cava and a part of blood sample was collected in EDTA tubes for blood cell counts (Red Blood cells (RBC), White Blood Cells (WBC) and Hemoglobin (Hb)). Plasma was separated from the rest of the blood samples by centrifugation for biochemistry assays and the level of aspartate aminotransferase (AST), alanine aminotransferase (ALT), lactate dehydrogenase (LDH), Blood Urea Nitrogen (BUN) and Creatinine (Cr) was determined by routine clinical laboratory techniques.

RESULTS

Effect of Cryoprotectant on NPs Freeze Drying

Freez drying is a process which is widely used for improving the stability of formulation. This process consists on removing water from a frozen sample under vacuum. Using cryoprotectant is a strategy to protect the formulation from stresses that generate during freeze drying Sugars are the most popular cryoprotectants that are encountered in the literature. (29). Different sugars (sucrose, glucose and mannitol) with various concentrations (0.5, 1, 2, 3, 4, 5% w/v) were used to examine the effect of presence or lack of cryoprotectants on the NPs characteristics.

In the absence of cryoprotectants, the NPs were aggregated and provided the collapsed appearance of particles which did not reconstitute easily. However, all formulations with cryoprotectant had fluffy cake in the same volume as the original frozen mass (Fig. 1a) which was reconstituted immediately after the addition of water by manual agitation.

Presence of sugars had no significant effect on zeta potential and EE of NPs (data not shown) but altered the size (Fig. 1b) and PDI (Fig. 1c) of NPs. Since the conservation of freeze dried product characteristics such as mean particle size and drug content are influence the freeze drying success and indicate an elegant processes, the ratio of size after and before freeze drying ($Size_{after}/Size_{before}$) as well as NPs size distribution (PDI_{after}/PDI_{before}) was evaluated in this study (29–31). If the ratio amount is near one it shows the conservations of NPs size wherease any elevation in this ratio more than value one represents the aggregation of NPs. As depicted in Fig. 1b, with all type of cryoprotectants, increasing the cryoprotectant concentration decreases the size ratio but at high concentrations it has an invert effect. In the presence of 0.5% w/v mannitol, the mean particle size after freeze drying was almost six fold more than mean particle size before freeze dying resulting in a $Size_{after}/Size_{before}$ ratio much greater than one . Similar trend was represented in the presence of sucrose. However, generally the $Size_{after}/Size_{before}$ ratio in presence of sucrose was less than the formulation with mannitol. The result of size

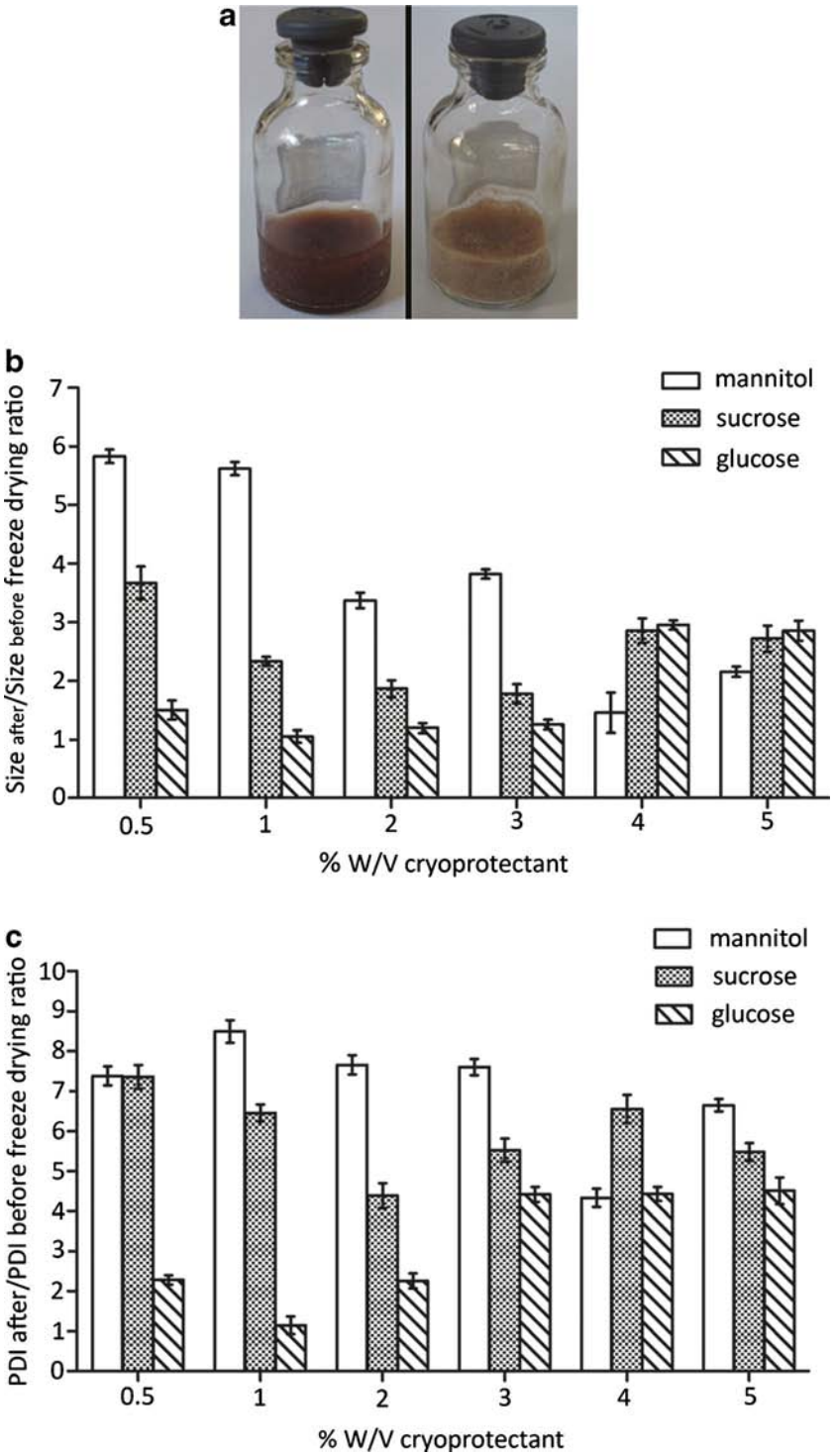

Fig. 1 (**a**) Vials filled by ZnPP-NPs formulations before (*left picture*) and after (*right picture*) freeze drying by addition of 1% w/v glucose as cryoprotectant. (**b**) Effect of different types of cryoprotectants with various concentrations on the size of NPs before and after freeze drying illustrated by means of $Size_{after}/Size_{before}$ ratio. (**c**) Ratio of NPs size polydispersity index (PDI) after freeze drying to before freeze dried product (PDI_{after}/PDI_{before}) in the presence of cryoprotectants with different concentrations.

distribution (PDI) measurements revealed that mannitol and sucrose were not able to conserve NP distribution as well as NP size (for all formulations, PDI more than 0.3 was observed) (Fig.1c). Only the addition of 1% w/v glucose, conserves the size of NPs very similar to original formulations with an acceptable PDI (0.116 ± 0.08). Formulation with this composition was used for further studies.

Experimental Design and Statistical Analysis

Experimental design was planned to determine the optimum experimental conditions for ZnPP-NPs preparation. Primary experiments were carried out in first step to select the factors effecting the NPs preparation and then in next step the selected factors were investigated to optimize NPs preparation conditions for obtaining NPs with maximum drug content while maintaining minimum mean particle size. The influence of the principal parameters of nanoprecipitation method on NPs characteristics was explored. For this purpose, different stirring rates (700, 900 and 1,200 rpm), different polymer concentration in the range of 5–40 mg/ml and different volumes of non-solvent volume in the range of 5–40 ml were screened in the preliminary study while keeping other parameters constant. Although changing the stirring speed was not a determinant factor for NP formation and their final characteristics, a too high polymer concentration (more than 30 mg/ml) resulted in large aggregates and prevented NP formation. This effect was probably due to the high viscosity of the polymer solution that impeded an appropriate diffusion of the solvent toward the non-solvent (32). Increasing the non-solvent volume from 5 to 40 ml influenced both the NP size and drug contents. Based on these studies, stirring rate kept constant at 900 rpm and the independent factors with appropriate levels were chosen for optimization studies.

In this study, the Box-Behnken design was carried out to optimize the preparation of PLGA NPs loaded with ZnPP by nanoprecipitation method. The individual and combined effect of PLGA amount (X1), ZnPP amount (X2) and non-solvent volume (X3) on mean particle size (Y1), EE (Y2) and DL (Y3) were investigated in 17 experiments. Each experiment was performed triplicate and the results are presented in Table II. The obtained NPs ranged from 78.3±8.39 to 125.9 ±11.01 nm in size with narrow size distribution (PDI<0.08) but there were significant changes in drug contents ranging from 33.4%±1.82 to 79.0%±2.19 for EE and from 2.32%± 0.539 to 9.59%±0.975 for DL.

The F-value of the model (32.5, 28.8 and 21.3 for mean particle size, EE and DL, respectively) indicated that models were significant. In all cases, the lack of fit test revealed that it was not significant relative to the pure error.

Analysis of variance (ANOVA) was further used to evaluate the significance of the variables and their interactions on the responses. Size and PDI of NPs were in acceptable pharmaceutical ranges so EE and DL was analyzed further. The variables having $P_{value}>0.05$ in the full model were discarded and the reduced models were generated. It produced the following quadratic equation showing the relationship between the responses and the variables in terms of coded factors:

$$EE = +49 + 10.62*(X1) - 6.35*(X2) - 11.32*(X3) + 7.23*(X1)^2$$

$$DL = +4.71 - 1.1*(X1) + 1.17*(X2) - 1.18*(X3) + 1.09*(X1)^2 - 0.85*(X2)^2 + 0.77(X1)*(X3)$$

According to ANOVA analysis and mathematical modeling, X1, X2, X3 and $X1^2$ were significant model terms ($P_{value}<0.05$) on EE. The predicted R-squared of 0.813 was in reasonable agreement with the adjusted R-squared of 0.874. It was also concluded that the experimental data and fitted model was in a good relationship based on R-squared value of 0.905 and adjusted R-squared value of 0.874. In terms of DL the P_{value} less than 0.05 was indicated that X1, X2, X3, $X1^2$ and the combination of X1 and X3 were significant effect. The relatively high R-squared (0.927) and adjusted R-squared (0.884) values implied a suitable relationship between the experimental data and those of the fitted model.

Response surface plots were prepared to analyze the optimum conditions for the dependent variables. As shown in Fig. 2a and b, an increase in non-solvent volumes results in a decrease in the drug content as a result of DMSO diffusion into non-solvent. Increasing the amount of polymer in the organic phase tends to increase the EE, (Fig. 2c) probably because a high concentration of polymer facilitates polymer precipitation and consequently, reduces drug leakage from emulsion droplets. From Fig. 2d, it can be concluded that a slight increase in polymer amount in constant amount of drug tended to increase DL. The amount of polymer and drug showed the quadratic effect on drug loading, so their effect on DL were influenced by interactions of variables and different mechanisms.

Optimization and Model Validation

Desirability functions were used for identification of the experimental conditions which resulted in the best responses. The scale of the desirability functions (D) ranges between D= 0 for a complete undesired response and D=1 for a fully desired response. For a value of 'D' close to 1, response values are near the target values (33). The condition of NP preparation with the highest overall desirability value, were used as optimum NPs in size, EE and DL. From Box-Behnken design and the experiments responses, it was found that all experiments had acceptable pharmaceutical size and PDI. Therefore for further studies in optimum model, the size was kept in the range and EE and DL were selected at their maximum level. Independent variables were optimized at polymer amount of 10 mg, drug amount of 1.52 mg and non-solvent volume of 5 ml. In this condition, dependent variables were predicted 106.6 nm, 58.8% and 8.41% for size, EE and DL respectively. For model validation and determination of prediction error, the nanoparticles were prepared experimentally with the predicted variables and were characterized (n=6). The observed responses were 100.12±

Table II Experiments Used in Box-Behnken Design and Their Results

Run	Independent variables			Dependent variable		
	X1 (mg)	X2 (mg)	X3 (ml)	Y1 (nm) (mean ± SD)	Y2 (mean ± SD)	Y3 (mean ± SD)
1	10	1.75	5	113.5 ± 12.67	64.3 ± 2.28	9.59 ± 0.975
2	17.5	1	40	93.3 ± 8.57	43.0 ± 2.45	2.32 ± 0.539
3	17.5	1.75	22.5	103.5 ± 12.86	48.7 ± 0.94	4.43 ± 0.864
4	10	1	22.5	85.6 ± 11.89	50.7 ± 2.73	4.61 ± 0.886
5	10	2.5	22.5	90.3 ± 13.66	33.4 ± 1.82	6.68 ± 1.032
6	17.5	1.75	22.5	108.1 ± 9.45	47.3 ± 1.34	4.30 ± 0.763
7	10	1.75	40	78.3 ± 8.39	33.9 ± 3.11	5.04 ± 1.302
8	17.5	2.5	40	104.4 ± 10.33	30.6 ± 1.94	3.83 ± 0.670
9	25	1.75	40	92.2 ± 13.53	56.3 ± 2.04	3.68 ± 0.962
10	17.5	1	5	123.1 ± 8.24	60.5 ± 1.90	3.27 ± 0.759
11	25	1	22.5	105.2 ± 7.50	71.5 ± 3.54	2.75 ± 0.941
12	17.5	1.75	22.5	112.8 ± 11.64	49.4 ± 2.86	4.49 ± 0.904
13	25	2.5	22.5	108.2 ± 11.85	60.6 ± 3.26	5.50 ± 0.792
14	17.5	1.75	22.5	117.3 ± 10.37	51.7 ± 1.37	4.70 ± 0.833
15	25	1.75	5	125.9 ± 11.01	79.0 ± 2.19	5.16 ± 0.938
16	17.5	1.75	22.5	122.6 ± 9.81	59.0 ± 1.28	5.36 ± 0.926
17	17.5	2.5	5	125.8 ± 9.76	50.4 ± 2.81	6.30 ± 0.852

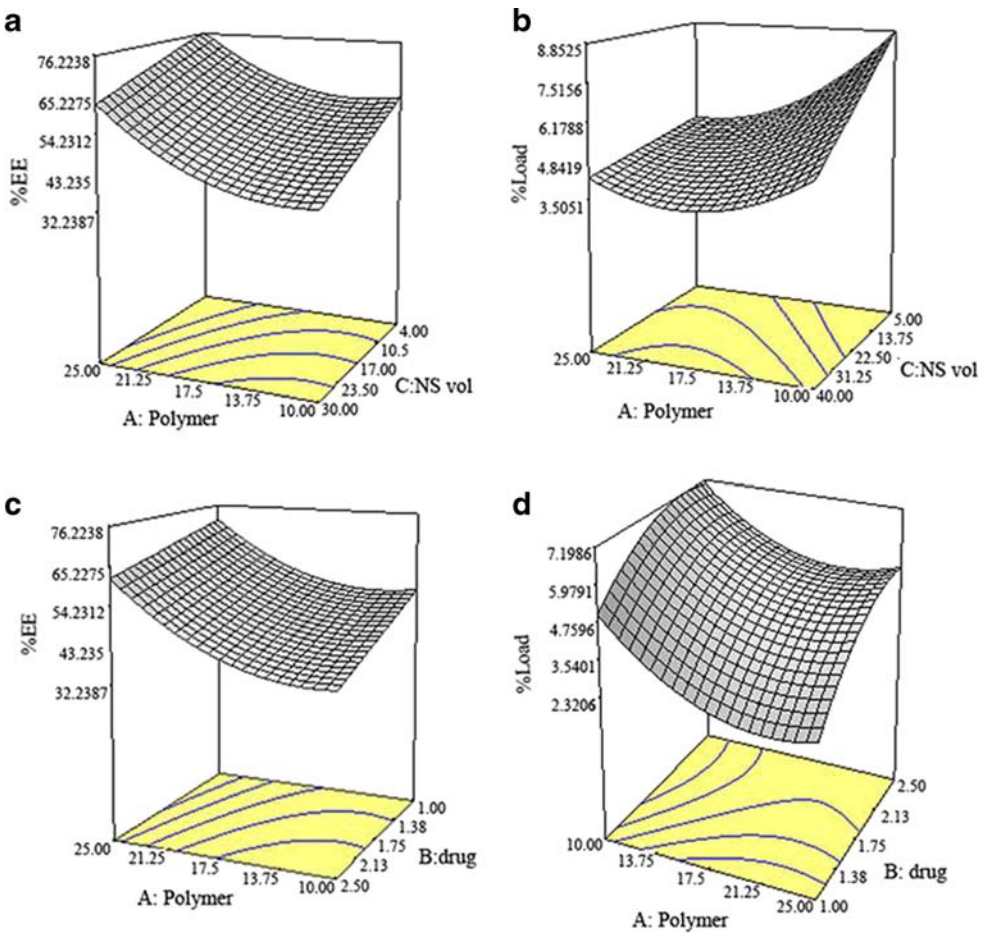

Fig. 2 The 3D response surface plot of (**a**) %EE and (**b**) %L variation with changes in non-solvent volume and polymer amount in constant amount of drug at 1.75 mg. (**c**) %EE and (**d**) %L variation with changes in polymer and drug amount, non-solvent volume was constant at 22.5 ml.

5.345 nm, 55.6%±2.49 and 7.98%±0.3412 for size, EE and DL respectively. The predicted value was in close agreement with the experimentally obtained value, suggesting that the applied model can indicate preparative conditions resulting in optimum NPs characteristics.

NPs Characterization

Optimized NPs showed average size, PDI and zeta potential of 100.12±5.345 nm, 0.064±0.041, -21.9±3.4 mV respectively with EE of 55.6%±2.49 and DL of 7.98%±0.341.

SEM was performed for morphologic observation of NPs in which, uniform particles having a diameter of 80–120 nm with suitable polydispersity was corroborated. NPs showed a spherical shape with smooth surfaces Fig. 3 illustrates the appearance of the NPs in two levels of magnification.

The *in vitro* ZnPP release rate from PLGA NPs was measured up to 4 days in pH 7.4 and 5.2. Figure 4 represents the biphasic release profile for NPs with an initial burst release during the first day, which was followed, by a sustained release. In the medium with pH 7.4 the drug release was almost 30% in the rapid release phase in first day followed by a slow release rate which remained constant even after 4 days and reached up to 45%. Although the whole

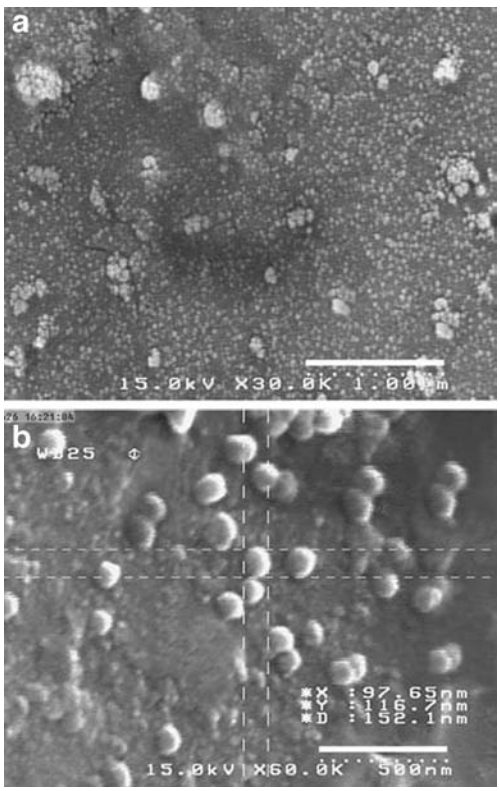

Fig. 3 Morphological evaluation of ZnPP loaded NPs by SEM images in different magnification levels (**a**) SEM image with 30× magnification level which presents the narrow distribution of NPs and (**b**) SEM image with 60× magnification level which presented the spherical particles with smooth surfaces.

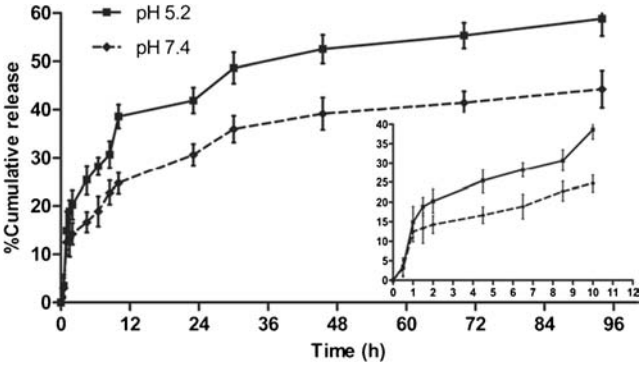

Fig. 4 The release behavior of ZnPP from the PLGA NPs in pH 7.4 (*black diamond suit*) and 5.2. (*black square*) to simulate the physiological condition and the lower pH condition of cancer cells. Each point shows mean ± SD ($n=3$).

percentage of drug release in pH 5.2 was higher than pH 7.4 (59% drug release after 4 days), the pattern of release was similar.

X-ray Diffraction (XRD)

Figure 5 plotted the XRD pattern of free ZnPP, PLGA, lyophilized ZnPP-NPs and physical mixture of ZnPP and PLGA. The presence of several distinct peaks in the XRD pattern of free ZnPP, at diffraction angles of $2\Theta = 6.85°$, 8.69°, 8.73° and 9.69° reveals the crystalline structure of ZnPP. Although PLGA pattern indicated the amorphous state of this polymer, in the physical mixture of ZnPP and PLGA the diffraction patterns of ZnPP was well consistent with that of free ZnPP. The sharp mentioned peaks of free ZnPP were not observed in the case of lyophilized ZnPP-NPs, which suggested the amorphous state of ZnPP entrapped into NPs.

In Vitro HO Inhibitory Effect

In biological media, hemin undergoes oxidative cleavage and degradation by HO enzyme to form biliverdin which is subsequently converted to bilirubin by biliverdin reductase (14). In this study, the liver cytosol (supernatant fraction of ultracentrifugation) and the spleen microsomes (pellet fraction of ultracentrifugation) were used as biliverdin reductase and HO enzyme sources respectively. In order to investigate the HO inhibitory activity of ZnPP-NPs in comparison with free ZnPP, the amount of decrease in bilirubin level as a product of the HO activity was examined. This was evaluated by the addition of hemin to the mixture of ZnPP-NPs, or free ZnPP with proteins and HO activity was studied in different preincubation times.

As plotted in Fig. 6a, the formation of bilirubin was decreased considerably in samples with ZnPP-NPs (1 μM equivalent ZnPP concentration) but it stayed constant in free ZnPP (1 μM) with different preincubation times. This is probably because of the time required for releasing the ZnPP from NPs.

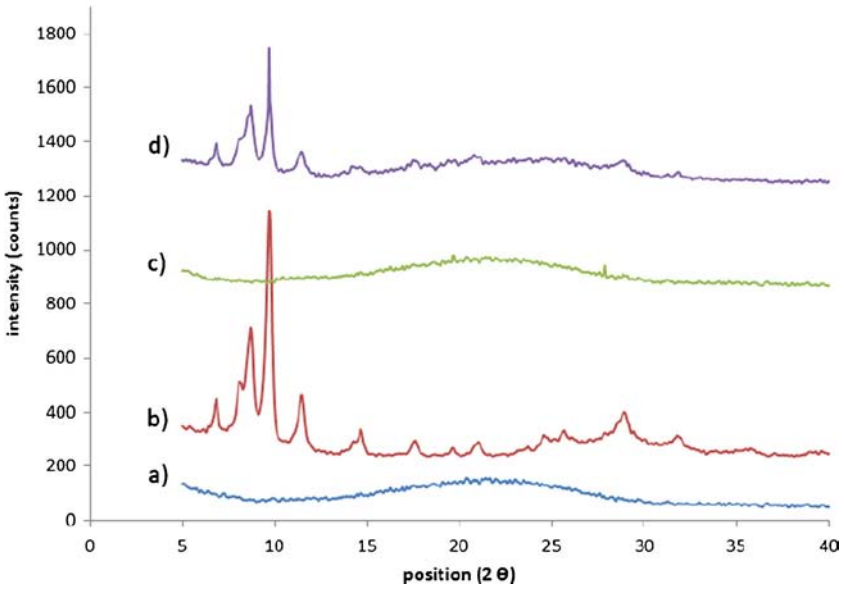

Fig. 5 Overlay of X-ray diffraction (XRD) patterns of *a*) PLGA, *b*) free ZnPP, *c*) ZnPP-NPs and *d*) physical mixture of ZnPP and PLGA.

The preincubation time of 90 min was used for further studies. To rule out the activity of entrapped ZnPP inside the NPs, HO inhibitory activity of free ZnPP and ZnPP-NPs (1 μM) were examined. In this experiment, HO inhibition was measured for $ZnCl_2$ and PLGA as blank sample and compared to samples without treatment as control. As depicted in Fig. 6b, neither $ZnCl_2$ nor PLGA as NPs components, showed inhibitory effects whereas ZnPP-NPs inhibited the HO enzyme activity similar to free ZnPP. Both free ZnPP and ZnPP-NPs resulted in approximately 45% reduction in heme oxidation level. This finding showed that the entrapped ZnPP inside the NPs maintains its functions and properties.

To determine the enzyme inhibition type and the effect of the inhibitors on the kinetics of HO enzyme, the Lineweaver–Burk plot was used (Fig. 7). K_m as the Michaelis-Menten constant, for hemin was measured to be 13.6 μM which is close to that reported previously (34). As seen in Fig. 7, free ZnPP and ZnPP-NPs inhibit the hemin degradation in a manner that shows the same y-intercept ($1/V_m$) but has different slopes and x-intercept ($-1/K_m$) in comparison with control, which represents a competitive inhibition. ZnPP in nanoparticle formulations with a k_i of approximately 0.2 μM showed the same kinetics of free ZnPP with a k_i of 0.15 μM.

Cellular Studies

In Vitro Cytotoxicity

In vitro cytotoxicity study of free ZnPP and ZnPP-NPs at a concentration range of 0.25 to 40 μM was analyzed by MTT assay on PC3, human prostate cancer cells. As shown in Fig. 8, cellular viability was decreased by increasing ZnPP concentration and incubation time. Figure 8a represents the cell viability after 24 h treatment with free ZnPP and ZnPP-NPs and Fig. 8b was plotted after 48 h incubation with samples. In PC3 cell line, the IC_{50} of free ZnPP was 7.54±0.032 μM, which is slightly lower than IC_{50} of ZnPP-NPs (9.56±0.195 μM) for 24 h incubation whereas the IC_{50} for 48 h incubation with free ZnPP and ZnPP-

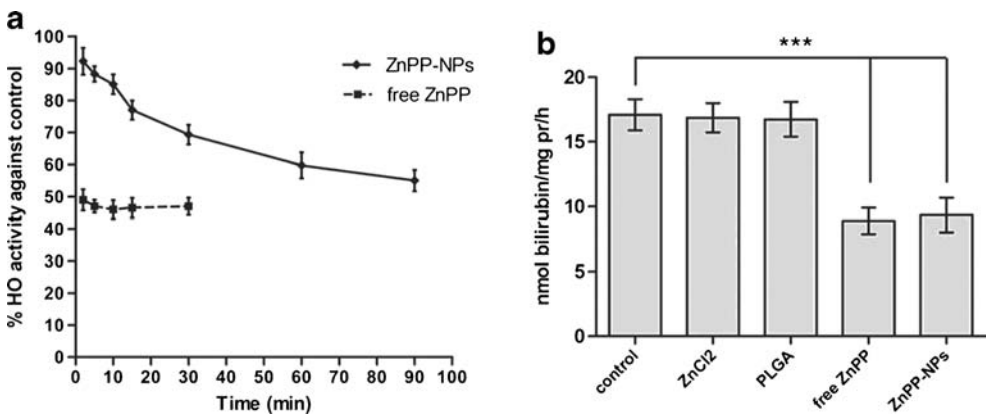

Fig. 6 (**a**) Effect of preincubation time on HO activity of free ZnPP (1 μM) and ZnPP-NPs (1 μM equivalent ZnPP concentration). Symbols: (■) as free ZnPP, (♦) as ZnPP-NPs. (**b**) The HO inhibitory effect of ZnPP-NPs in comparison with, free ZnPP, $ZnCl_2$, PLGA and control. *** Significantly different from control group with $P_{value} < 0.001$.

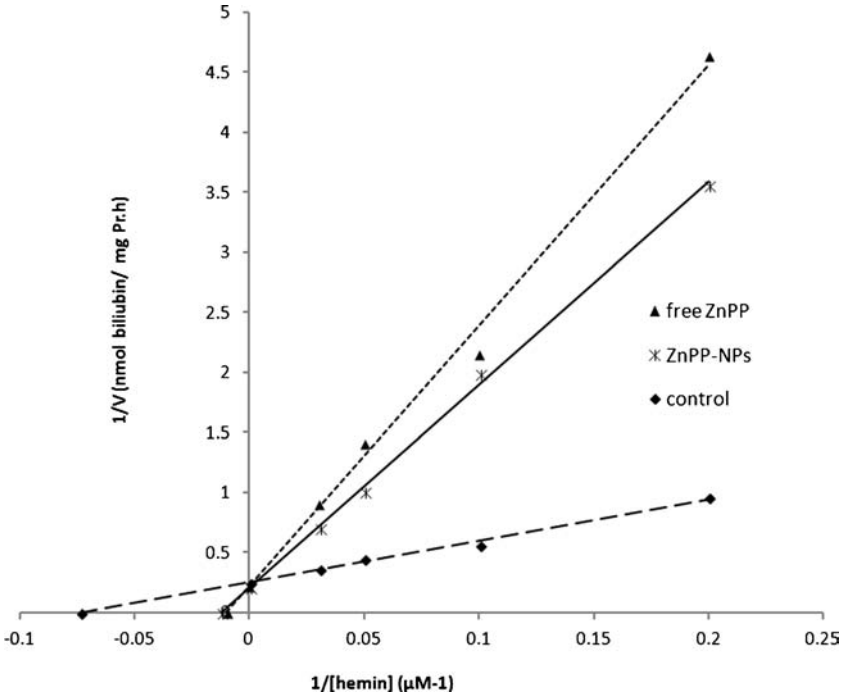

Fig. 7 The Lineweaver-Burk plot of HO inhibitory effect based on the effect of ZnPP-NPs and free ZnPP on the oxidation of hemin as the substrate *versus* control, Symbols: (*black up-pointing triangle*) as free ZnPP, (*asterisk*) as ZnPP-NPs and (*black diamond suit*) as control.

NPs were 2.58±0.145 and 2.142±0.08 μM, respectively. These results elicited that free ZnPP showed more cytotoxicity than ZnPP-NPs in 24 h; however at 48 h, the cytotoxicity of NPs formulations increased even more than free ZnPP because of the release of ZnPP from NPs into the cells (Table III).

As shown in Fig. 9, comparing cell viability of various formulations of ZnPP with 5 μM concentration of ZnPP beside vehicle and blank NPs after 24 and 48 h incubation indicated that cell viability of vehicle and blank NPs were more than 90%, which demonstrated no toxicity had occurred by them. It was also concluded that the ZnPP-NPs formulations could achieve higher toxicity after 48 h compared to free ZnPP as a result of drug release from NPs.

In Vitro Cellular Uptake

It is clear that the therapeutic effect of NPs depends on their internalization by cancer cells. Therefore, the *in vitro* investigation can provide evidences to show the cellular uptake of NPs. The properties of coumarin-6 have made it one of the useful compounds in cellular uptake study, based on its high fluorescent activity beside low leakage rate from NPs formulation (35).

Figure 10a demonstrated that the NPs had been indeed internalized in the cell and the cellular uptake was increased with the longer incubation time. The quantitative cellular uptake after 0.5, 1, 2 and 4 h was measured 16.5%±2.57, 21.3%±1.63, 30.8%±2.29 and 45.8%±2.54, respectively. This internalization was confirmed by CLSM image after 4 h incubation of PC3 cells with coumarin-6 loaded NPs (Fig. 10b). As it can be seen in this figure, the fluorescence intensity of coumarin-6 is distributed in cytoplasm.

In Vivo Studies

Biodistribution Assay

The goal of the biodistribution studies was to investigate differences in organ distribution of ZnPP-NPs compared to

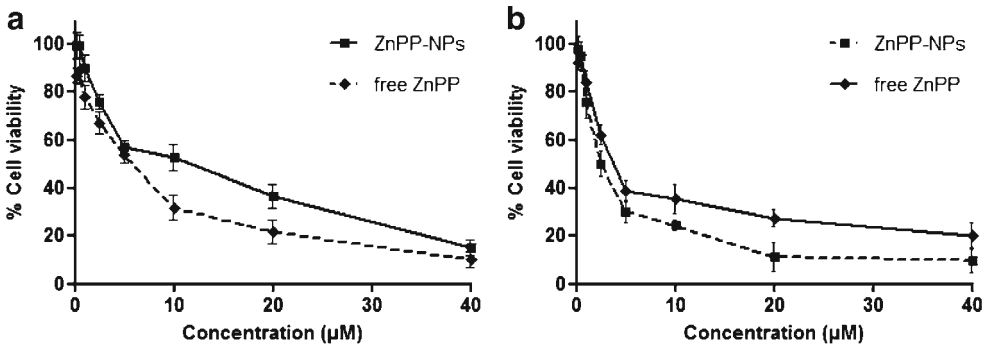

Fig. 8 *In vitro* cytotoxic effect of ZnPP-NPs and free ZnPP on PC3 cell line. (**a**) after 24 h and (**b**) after 48 h incubation time. Symbols: (*black square*) as ZnPP-NPs and (*black diamond suit*) as free ZnPP.

Table III IC_{50} Value of Free ZnPP and ZnPP-NPs on PC3 Cell Line. Cell Viability Was Determined by Means of the MTT Assay. Values are Mean ± SD ($n=6$)

Sample	$IC_{50}\mu M$(24 h)	$IC_{50}\mu M$ (48 h)
Free ZnPP	7.54 ± 0.032	2.58 ± 0.145
ZnPP-NPs	9.56 ± 0.195	2.14 ± 0.083

free ZnPP The resulted data at 4, 8, 24 and 48 h post i.v. injection of the formulations was illustrated in Fig. 11. In general, it was observed that the tissue concentrations were highest in liver and spleen for both formulations at all times. ZnPP entrapping could not change the distribution amount of ZnPP to kidneys, heart and intestine ($P_{value}>0.05$) in comparison with free ZnPP. In the case of ZnPP-NPs, the accumulation of NPs in lungs was higher than free ZnPP, possibly due to the filtration effect of the lung capillary bed that removes some large particles of the aggregates (36,37).

Evaluation of formulations distribution in a manner of time shows that at the early times, only the minor part of free ZnPP was detected in blood (6.2% ± 2.88) and other organs excluding liver (25.7% ± 3.29) and spleen (29.5% ± 5.68). Free ZnPP was removed from blood and was accumulated more in liver then excreted in kidney during the time. For all times, plasma level of ZnPP was higher for NPs compared to free ZnPP in a way that the plasma level in 4 h was 6.2% ± 2.88 for free ZnPP *versus* 13.2% ± 2.87 for ZnPP-NPs and it was maintained at acceptable level of 12.7% ± 1.96 for 8 h and 6.9% ± 1.09 for 24 h. NPs showed longer circulation times in blood while free ZnPP plasma level was dropped rapidly after the first 4 h. During time, NPs showed the same fate as free ZnPP and were accumulated in liver until excreted.

In Vivo Blood Cytotoxicity/Hematological Toxicity

The major susceptible organs to nonspecific HO inhibition are liver, spleen and bone marrow. The body distribution

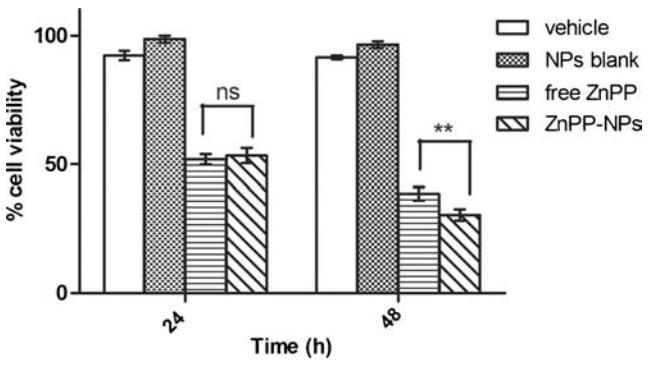

Fig. 9 *In vitro* viability of PC3 cell line treated with blank NPs, vehicle, free ZnPP and ZnPP-NPs at 5 μM ZnPP equivalent concentration, after 24 and 48 h incubation time ($n=6$). ns: not significatly different,**: significantly different from free ZnPP and ZnPP-NPs with $P_{value}<0.01$.

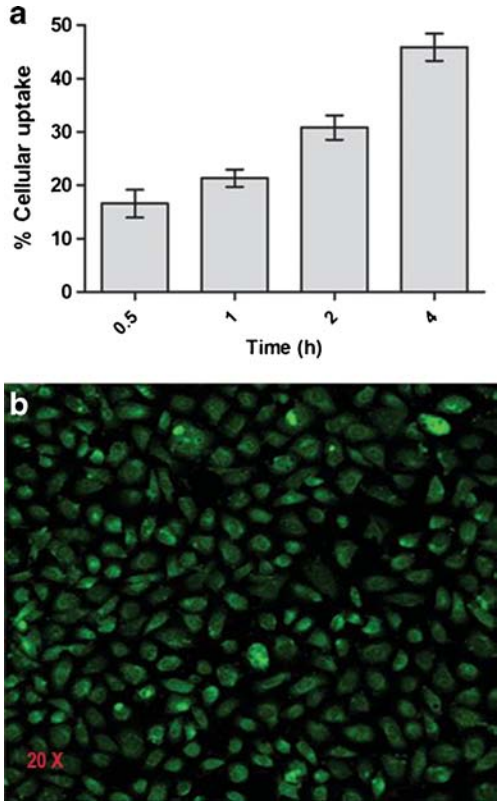

Fig. 10 (**a**) Cellular uptake of coumarin-6 loaded NPs after 0.5, 1, 2, 4 h incubation at 1.25 μg/ml coumarin-6 concentration by PC3 cells. Fluorescent intensity of coumarin-6 was measured by microplate reader using $\lambda_{excitation}=470$ nm and $\lambda_{emission}=520$ nm. (**b**) Confocal Laser Scanning Microscopy (CLSM) of PC3 cells after 4 h incubation with coumarin-6 loaded NPs with 20× magnification level.

studies also confirm this finding. So the blood chemistry and blood cell counts were assessed to investigate the hematological toxicity against NPs. As shown in Table IV, one way ANOVA statistical test showed that there is no significant differences ($P_{value}>0.05$) in WBC, RBC and Hb count in addition to AST, ALT, LDH, BUN and Cr values in 24 and 48 h after ZnPP-NPs administration compared to control groups. According to the acquired results, it was evident that no toxic effect by ZnPP-NPs on major normal organs.

DISCUSSION

The present study demonstrates the preparation and development of ZnPP encapsulated PLGA NPs and investigates the ZnPP-NPs characteristics in addition to their *in vitro* cytotoxicity and HO inhibitory effect as well as their *in vivo* biodistribution and blood toxicity.

In order to achieve a physico-chemical stable NPs formulation, water must be removed from the system. In this regard, the most common process which is used for long term storage of products is freeze drying. However this process generates various

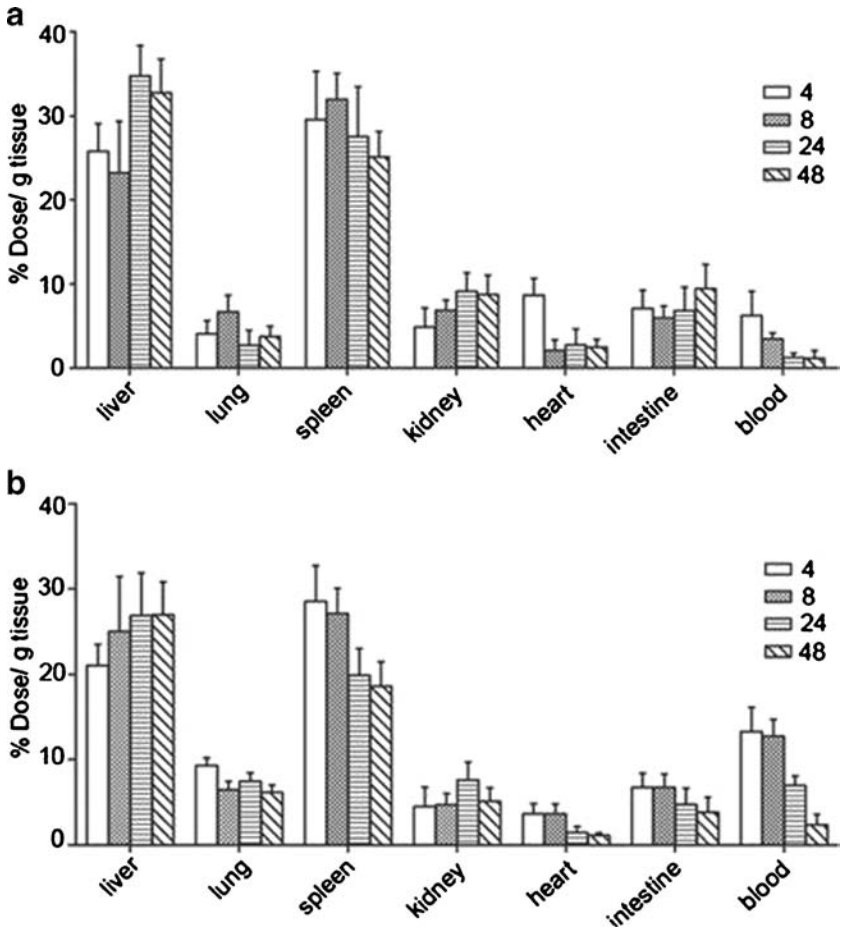

Fig. 11 Biodistribution of (**a**) free ZnPP, (**b**) ZnPP-NPs containing 5 mg/kg ZnPP at 4, 8, 24 and 48 h following 0.15 ml i.v. injection in balb/c mice. Presence of ZnPP in various organs was meatured by spectrofluorophotometry at $\lambda_{ecitation} = 420$ nm and $\lambda_{emission} = 590.4$ nm. Each point shows mean ± SD for 5 mice.

stresses, especially during freezing and dehydration steps. Moreover, the lack of surfactants in the nanoprecipitation method can cause aggregation of NPs. As a results protectants utilization can be a useful strategy to prevent such complication (29,38). An aggregated and collapsed cake which are usually formed after freeze drying process without cryoprotectants, are not acceptable and con not be used after reconstitution. The success of freeze drying is defined by various parameters consisting of rapid reconstitution time, long term stability and conservation of the freeze dried product characteristics (small or unmodified NP size and drug entrapment) (29). To gain this purpose, the different sugars (sucrose, glucose and mannitol) with various concentrations were investigated and the proper type of cryoprotectant and its concentration was selected based on mentioned parameters. In order to indicate the effect of freeze drying process on NPs properties, after to before size and PDI ratio as well as zeta potential and EE ratio was measured. In presence of mannitol and sucrose the size and PDI of NPs were not preserved regardless of the freeze drying process. Addition of 1% w/v glucose to NPs suspension conserved the size of NPs similar to the size before freeze drying and resulted to a better cake.

Table IV Blood Cell Counts (RBC, WBC, Hb) and AST, ALT Enzymes, LDH, BUN and Cr Level in Balb/c Mice Treated with ZnPP-NPs *Versus* Control Group. Values are Presented as Mean ± SD ($n = 3$)

Assays	Sample	Control	ZnPP-NPs (24 h)	ZnPP-NPs (48 h)
Blood cell counts	WBC (1,000/μl)	2.7 ± 0.63	3.9 ± 2.03	3.5 ± 1.03
	RBC (mil/ul)	10.1 ± 0.82	10.6 ± 0.65	9.8 ± 0.96
	Hb (g/dL)	14.4 ± 1.62	14.4 ± 1.13	13.9 ± 0.07
Biochemistry	AST (IU/L)	295.0 ± 24.04	304.3 ± 39.59	214.2 ± 33.23
	ALT (IU/L)	49.1 ± 4.24	59.2 ± 8.48	60.5 ± 9.89
	LDH (IU/L)	993.8 ± 220.61	1,164.8 ± 251.73	1,034.7 ± 119.55
	BUN (mg/dL)	49.5 ± 2.12	42.3 ± 1.41	51.5 ± 4.24
	Cr (mg/dL)	0.5 ± 0.01	0.5 ± 0.02	0.5 ± 0.07

Experimental design has an important role in modern researches and development efforts. Proper experimental design techniques consider all factors and their interactions, which is in contrary with the time consuming classical univariate approach (39). A primary study was carried out to determine the main factors and their levels subsequently to decrease the number of independent variables and experiments. Box-Behnken design was applied to optimize the level of the selected variables including polymer amount, drug amount and non-solvent volume on size, EE and DL. Figure 2 represents the effect of variables on drug content of NPs. According to the NP formation mechanism in nanoprecipitation method, an increase in non-solvent volume would facilitate the diffusion of DMSO as a solvent into the non-solvent, which consequently increases the solubility of ZnPP in water and causes ZnPP leakage from NP to the aqueous phase (32). It was shown that increasing the amount of polymer facilitates polymer precipitation and consequently increases %EE. When the drug amount kept constant, DL was also enhanced by increasing the polymer amount. The amount of polymer and drug showed a quadratic effect on drug loading, so their effect on DL was influenced by interactions of variables and different mechanisms. Based on Box-Behnken design, the optimized formulation was prepared and the optimized NPs were further investigated.

The drug release mechanism could be referred to drug diffusion, polymer matrix and polymer erosion or degradation. In this study, the release pattern of NPs in pH 7.4 and 5.2 was similar. However the whole percentage of drug release was found to be dependent on the pH of the incubation medium. The fraction of initial burst drug released was probably because of the superficially attached drug molecules (40,41). The slow release rate was also expected because of high hydrophobicity nature of ZnPP, which prevented the drug diffusion from PLGA matrix into aqueous medium (41). The pH effect was correlated to the PLGA degradation degree in acidic medium. This was expected because of the degradation due to hydrolytic cleavage of the ester linkage (26). The slow release of ZnPP at biological pH assures the NP stability during circulation which may necessitate less frequent drug administration.

In order to investigate the physical state of ZnPP in NPs, XRD study was examined. The state of drug which was incorporated inside the NPs could influence the *in vitro* and *in vivo* release profile of drug (42). The XRD pattern of ZnPP-NPs in comparison with free ZnPP, PLGA and physical mixture of them, revealed that the ZnPP was incorporated inside the NPs in an amorphous state.

ZnPP encapsulation in NPs did not affect the ZnPP HO inhibitory potential. ZnPP-NPs inhibited the HO enzyme activity in a competitive manner which was similar to free ZnPP. *In vitro* cytotoxicity experiments showed that ZnPP-NPs had cytotoxic effect on PC3 human prostate cancer cell line. NPs showed the higher cytotoxicity after 48 h incubation time in comparison to free ZnPP as which may be due to drug release from NPs. Nevertheless the release rate of ZnPP from NPs was found to be slow, the cytotoxicity of NPs was identical and even higher after 48 h as that of free ZnPP. One possible explanation to this marked cytotoxicity may be the efficient cellular uptake of the NPs into cells (17). Internalization of NPs by PC3 cells was studied on coumarin-6 loaded NPs which showed the distribution of NPs in cytoplasm of cells.

Biodistribution study demonstrated that the tissue concentration of ZnPP was highest in liver and spleen for both NPs formulation and free ZnPP. Since these two sites are considered as the major organs possessing an active Reticulo Endothelial System (RES) as well as a high level of endogenous HO-1, these results are reasonable. It has been found that the surface of the ZnPP-NPs was not hydrophilic enough to bypass the RES macrophages completely and more surface treatment is required (38). Further study on distribution of these formulations in tumor tissue may be expletive. Blood concentration of NPs remained at an acceptable level up to 24 h in comparison to free ZnPP that showed longer blood circulation time. The intrinsic anti-oxidants level of liver as well as normal cells was high enough to prevent inhibition of HO by ZnPP (11). This finding was proved by *in vivo* blood cytotoxicity assays. No toxic effects by ZnPP were found on liver, spleen and blood cell count as major organs.

The non-specific inhibition of HO may cause various side effects in normal cells by reducing the favorable effects of normal anti-oxidants (11,23). In this regard, necessity of efficient delivery of HO inhibitors to tumor tissue is inevitable.

CONCLUSION

In the present work, ZnPP loaded PLGA nanoparticles were successfully prepared by nanoprecipitation method. This technique is rapid, easy to perform and is carried out in one-step. Moreover, no surfactants are needed in this method (43). The size of NPs in addition to entrapment efficiency and drug loading were controlled by accurate selection of optimal formulation conditions according to the Box-Behnken design based on three independent variables. The optimized formulation was further characterized. The NPs size measurements demonstrated a homogenous population characterized by narrow size distribution which were proved by SEM images. Furthermore, the drug content by the means of entrapment efficiency and drug loading beside release behavior of NPs were investigated. The NPs were readily resuspended in aqueous solution after freeze drying without significant modification of their size and PDI. ZnPP entrapment in PLGA NPs did not influence the HO inhibitory kinetics of ZnPP and the NPs exhibited potent cytotoxic effects on PC3 human prostate

cancer cell lines as well as high cellular uptake. Collectively, it is assumed that the overall process could become a good candidate for encapsulation of ZnPP as a potent HO inhibitor for cancer treatment. Further study on distribution of these formulations in tumor tissue may be expletive. Moreover, necessity of efficient delivery of HO inhibitors to tumor tissue is inevitable.

ACKNOWLEDGMENTS AND DISCLOSURES

Authors would like to express their profound thanks to Mr. A.R. Kazemi for his technical assistance in animal experiments. This work is a part PhD thesis of first author and was financially supported by a grant from Tehran University of Medical Sciences.

REFERENCES

1. Haley B, Frenkel E, editors. Nanoparticles for drug delivery in cancer treatment. Urol Oncol: Seminars and original investigations. Elsevier; 2008.
2. Sanvicens N, Marco MP. Multifunctional nanoparticles–properties and prospects for their use in human medicine. Trends Biotechnol. 2008;26(8):425–33.
3. Oberley TD. Oxidative damage and cancer. Am J Pathol. 2002;160(2):403.
4. Poli G, Leonarduzzi G, Biasi F, Chiarpotto E. Oxidative stress and cell signalling. Curr Med Chem. 2004;11(9):1163–82.
5. Gupte A, Mumper RJ. Elevated copper and oxidative stress in cancer cells as a target for cancer treatment. Cancer Treat Rev. 2009;35(1):32–46.
6. Valko M, Izakovic M, Mazur M, Rhodes CJ, Telser J. Role of oxygen radicals in DNA damage and cancer incidence. Mol Cell Biochem. 2004;266(1–2):37–56.
7. Kondo S, Toyokuni S, Iwasa Y, Tanaka T, Onodera H, Hiai H, *et al.* Persistent oxidative stress in human colorectal carcinoma, but not in adenoma. Free Radic Biol Med. 1999;27(3):401–10.
8. Was H, Dulak J, Jozkowicz A. Heme oxygenase-1 in tumor biology and therapy. Curr Drug Targets. 2010;11(12):1551–70.
9. Pervaiz S, Clement M-V. Tumor intracellular redox status and drug resistance-serendipity or a causal relationship. Curr Pharm Des. 2004;10(16):1969–77.
10. Powis G, Gasdaska JR, Baker A. Redox signaling and the control of cell growth and death. Adv Pharmacol. 1996;38:329–59.
11. Fang J, Seki T, Maeda H. Therapeutic strategies by modulating oxygen stress in cancer and inflammation. Adv Drug Deliv Rev. 2009;61(4):290–302.
12. Sawa T, Wu J, Akaike T, Maeda H. Tumor-targeting chemotherapy by a xanthine oxidase-polymer conjugate that generates oxygen-free radicals in tumor tissue. Cancer Res. 2000;60(3):666–71.
13. Fang J, Sawa T, Akaike T, Maeda H. Tumor-targeted delivery of polyethylene glycol-conjugated D-amino acid oxidase for antitumor therapy via enzymatic generation of hydrogen peroxide. Cancer Res. 2002;62(11):3138–43.
14. Kinobe RT, Dercho RA, Nakatsu K. Inhibitors of the heme oxygenase-carbon monoxide system: on the doorstep of the clinic. Can J Physiol Pharmacol. 2008;86(9):577–99.
15. Fang J, Akaike T, Maeda H. Antiapoptotic role of heme oxygenase (HO) and the potential of HO as a target in anticancer treatment. Apoptosis. 2004;9(1):27–35.
16. Sahoo S, Sawa T, Fang J, Tanaka S, Miyamoto Y, Akaike T, *et al.* Pegylated zinc protoporphyrin: a water-soluble heme oxygenase inhibitor with tumor-targeting capacity. Bioconjug Chem. 2002;13(5):1031–8.
17. Fang J, Sawa T, Akaike T, Akuta T, Sahoo SK, Khaled G, *et al.* In vivo antitumor activity of Pegylated zinc protoporphyrin targeted inhibition of heme oxygenase in solid tumor. Cancer Res. 2003;63(13):3567–74.
18. Fang J, Sawa T, Akaike T, Greish K, Maeda H. Enhancement of chemotherapeutic response of tumor cells by a heme oxygenase inhibitor, pegylated zinc protoporphyrin. Int J Cancer. 2004;109(1):1–8.
19. Iyer AK, Greish K, Fang J, Murakami R, Maeda H. High-loading nanosized micelles of copoly (styrene–maleic acid)–zinc protoporphyrin for targeted delivery of a potent heme oxygenase inhibitor. Biomaterials. 2007;28(10):1871–81.
20. Iyer AK, Greish K, Seki T, Okazaki S, Fang J, Takeshita K, *et al.* Polymeric micelles of zinc protoporphyrin for tumor targeted delivery based on EPR effect and singlet oxygen generation. J Drug Target. 2007;15(7–8):496–506.
21. Regehly M, Greish K, Rancan F, Maeda H, Böhm F, Röder B. Water-soluble polymer conjugates of ZnPP for photodynamic tumor therapy. Bioconjug Chem. 2007;18(2):494–9.
22. Ding H, Sumer BD, Kessinger CW, Dong Y, Huang G, Boothman DA, *et al.* Nanoscopic micelle delivery improves the photophysical properties and efficacy of photodynamic therapy of protoporphyrin IX. J Control Release. 2011;151(3):271–7.
23. Fang J, Nakamura H, Iyer A. Tumor-targeted induction of oxystress for cancer therapy. J Drug Target. 2007;15(7–8):475–86.
24. Byrne JD, Betancourt T, Brannon-Peppas L. Active targeting schemes for nanoparticle systems in cancer therapeutics. Adv Drug Deliv Rev. 2008;60(15):1615–26.
25. Davis ME. Nanoparticle therapeutics: an emerging treatment modality for cancer. Nat Rev Drug Discov. 2008;7(9):771–82.
26. Dinarvand R, Sepehri N, Manoochehri S, Rouhani H, Atyabi F. Polylactide-co-glycolide nanoparticles for controlled delivery of anticancer agents. Int J Nanomedicine. 2011;6:877.
27. Maines MD. Zinc protoporphyrin is a selective inhibitor of heme oxygenase activity in the neonatal rat. Biochim et Biophys Acta (BBA)-General Subjects. 1981;673:339–50.
28. Drummond GS, Kappas A. Prevention of neonatal hyperbilirubinemia by tin protoporphyrin IX, a potent competitive inhibitor of heme oxidation. Proc Natl Acad Sci. 1981;78(10):6466–70.
29. Abdelwahed W, Degobert G, Stainmesse S, Fessi H. Freeze-drying of nanoparticles: formulation, process and storage considerations. Adv Drug Deliv Rev. 2006;58(15):1688–713.
30. Saez A, Guzman M, Molpeceres J, Aberturas M. Freeze-drying of polycaprolactone and poly (D, L-lactic-glycolic) nanoparticles induce minor particle size changes affecting the oral pharmacokinetics of loaded drugs. Eur J Pharm Biopharm. 2000;50(3):379–87.
31. Bozdag S, Dillen K, Vandervoort J, Ludwig A. The effect of freeze-drying with different cryoprotectants and gamma-irradiation sterilization on the characteristics of ciprofloxacin HCl-loaded poly (D, L-lactide-glycolide) nanoparticles. J Pharm Pharmacol. 2005;57(6):699–707.
32. Bilati U, Allémann E, Doelker E. Development of a nanoprecipitation method intended for the entrapment of hydrophilic drugs into nanoparticles. Eur J Pharm Sci. 2005;24(1):67–75.
33. Deming SN. Multiple-criteria optimization. J Chromatogr A. 1991;550:15–25.
34. Maines MD, Kappas A. Cobalt stimulation of heme degradation in the liver. Dissociation of microsomal oxidation of heme from cytochrome P-450. J Biol Chem. 1975;250(11):4171–7.

35. Sun B, Ranganathan B, Feng S-S. Multifunctional poly (d, l-lactide-co-glycolide)/montmorillonite (PLGA/MMT) nanoparticles decorated by Trastuzumab for targeted chemotherapy of breast cancer. Biomaterials. 2008;29(4):475–86.
36. Esmaeili F, Dinarvand R, Ghahremani MH, Ostad SN, Esmaily H, Atyabi F. Cellular cytotoxicity and in-vivo biodistribution of docetaxel poly (lactide-co-glycolide) nanoparticles. Anticancer Drugs. 2010;21(1):43–52.
37. Jin C, Bai L, Wu H, Song W, Guo G, Dou K. Cytotoxicity of paclitaxel incorporated in PLGA nanoparticles on hypoxic human tumor cells. Pharm Res. 2009;26(7):1776–84.
38. Cheng J, Teply BA, Sherifi I, Sung J, Luther G, Gu FX, *et al.* Formulation of functionalized PLGA–PEG nanoparticles for in vivo targeted drug delivery. Biomaterials. 2007;28(5):869–76.
39. Hao J, Fang X, Zhou Y, Wang J, Guo F, Li F, *et al.* Development and optimization of solid lipid nanoparticle formulation for ophthalmic delivery of chloramphenicol using a Box-Behnken design. Int J Nanomedicine. 2011;6:683.
40. Sabzevari A, Adibkia K, Hashemi H, Hedayatfar A, Mohsenzadeh N, Atyabi F, *et al.* Polymeric triamcinolone acetonide nanoparticles as a new alternative in the treatment of uveitis: In vitro and in vivo studies. Eur J Pharm Biopharm. 2013.
41. Mu L, Feng S-S. PLGA/TPGS nanoparticles for controlled release of paclitaxel: effects of the emulsifier and drug loading ratio. Pharm Res. 2003;20(11):1864–72.
42. Zhang L, Yang M, Wang Q, Li Y, Guo R, Jiang X, *et al.* 10-Hydroxycamptothecin loaded nanoparticles: preparation and antitumor activity in mice. J Control Release. 2007;119(2):153–62.
43. Vauthier C, Bouchemal K. Methods for the preparation and manufacture of polymeric nanoparticles. Pharm Res. 2009;26(5):1025–58.